

John C. Russ

Image Analysis *of* Food Microstructure



CRC PRESS

Image Analysis
of
Food
Microstructure

Image Analysis *of* Food Microstructure

John C. Russ



CRC PRESS

Boca Raton London New York Washington, D.C.

Library of Congress Cataloging-in-Publication Data

Russ, John C.

Image analysis of food microstructure / John C. Russ.

p. cm.

Includes index.

ISBN 0-8493-2241-3 (alk. paper)

1. Food—Analysis. 2. Microscopy. 3. Image analysis. I. Title.

TX543.R88 2004

664'.07—dc22

2004051958

This book contains information obtained from authentic and highly regarded sources. Reprinted material is quoted with permission, and sources are indicated. A wide variety of references are listed. Reasonable efforts have been made to publish reliable data and information, but the author and the publisher cannot assume responsibility for the validity of all materials or for the consequences of their use.

Neither this book nor any part may be reproduced or transmitted in any form or by any means, electronic or mechanical, including photocopying, microfilming, and recording, or by any information storage or retrieval system, without prior permission in writing from the publisher.

The consent of CRC Press LLC does not extend to copying for general distribution, for promotion, for creating new works, or for resale. Specific permission must be obtained in writing from CRC Press LLC for such copying.

Direct all inquiries to CRC Press LLC, 2000 N.W. Corporate Blvd., Boca Raton, Florida 33431.

Trademark Notice: Product or corporate names may be trademarks or registered trademarks, and are used only for identification and explanation, without intent to infringe.

Visit the CRC Press Web site at www.crcpress.com

© 2005 by CRC Press LLC

No claim to original U.S. Government works

International Standard Book Number 0-8493-2241-3

Library of Congress Card Number 2004051958

Printed in the United States of America 1 2 3 4 5 6 7 8 9 0

Contents

| | | |
|------------------|---|-----|
| Chapter 1 | Stereology | 1 |
| | The Need for Stereology | 1 |
| | Unfolding Size Distributions..... | 5 |
| | Volume Fraction..... | 11 |
| | Surface Area..... | 21 |
| | Lines and Points | 28 |
| | Design of Experiments | 31 |
| | Topological Properties | 34 |
| | Other Stereological Techniques..... | 41 |
| | | |
| Chapter 2 | Image Acquisition | 51 |
| | Scanners | 51 |
| | Digital Cameras | 57 |
| | Scanning Microscopes | 63 |
| | File Formats | 67 |
| | Color Adjustment..... | 71 |
| | Color Space Coordinates | 77 |
| | Color Channels | 81 |
| | Optimum Image Contrast | 86 |
| | Removing Noise | 98 |
| | Nonuniform Illumination..... | 111 |
| | Image Distortion and Focus | 121 |
| | Summary | 127 |
| | | |
| Chapter 3 | Image Enhancement | 129 |
| | Improving Local Contrast..... | 131 |
| | Image Sharpening | 135 |
| | False Color and Surface Rendering | 142 |
| | Rank-Based Filters | 145 |
| | Edge-Finding..... | 147 |
| | Texture | 156 |
| | Directionality | 164 |
| | Finding Features in Images | 169 |
| | Image Combinations..... | 175 |
| | Thresholding | 184 |
| | Automatic Threshold Settings Using the Histogram..... | 189 |
| | Automatic Thresholding Using the Image..... | 197 |

| | |
|---|-----|
| Other Thresholding Approaches..... | 200 |
| Color Image Thresholding..... | 205 |
| Manual Marking | 209 |
| Summary | 211 |
| Chapter 4 Binary Images | 213 |
| Erosion and Dilation..... | 213 |
| The Euclidean Distance Map | 219 |
| Separating Touching Features | 223 |
| Boolean Combinations | 236 |
| Using Grids for Measurement..... | 240 |
| Using Markers to Select Features | 247 |
| Combined Boolean Operations | 250 |
| Region Outlines as Selection Criteria | 252 |
| Skeletonization..... | 254 |
| Fiber Images | 260 |
| Skeletons and Feature Shape..... | 262 |
| Measuring Distances and Locations with the EDM..... | 263 |
| Summary | 275 |
| Chapter 5 Measuring Features | 277 |
| Counting..... | 277 |
| Calibration..... | 287 |
| Size Measurement..... | 292 |
| Size Distributions..... | 297 |
| Comparisons | 301 |
| Edge Correction..... | 303 |
| Brightness and Color Measurements | 310 |
| Location | 316 |
| Gradients | 324 |
| Shape..... | 342 |
| Identification | 350 |
| Conclusions..... | 359 |
| Index | 361 |

Introduction

Why is a book about food microstructure written by someone with a background in engineering materials?

My own path to recognizing the importance of image analysis to measure microstructural parameters in food products has been round-about. For nearly two decades as a professor in the Materials Science and Engineering Department at North Carolina State University I taught a sophomore course in basic materials science that included such fundamentals as mechanical properties of metals, ceramics, polymers and composites and the procedures for testing them, the basics of phase diagrams and the formation of microstructures during phase transformations, and so on. Because many of the students came into the course with little background in materials, but with about 20 years of experience in eating, I commonly used food examples to explain various processes. College students generally respond well to comparisons of using the liquid-solid phase change to produce ice beer versus the liquid-gas phase change to distill corn liquor. Other examples used cooked spaghetti as a model for the entanglement of linear polymers, and fruit in Jell-O as a model for dispersion strengthening.

Little did I realize at the time that the people whose products are food would look to materials for models of behavior. It was only recently that I discovered in the excellent text by Aguilera and Stanley (*Microstructural Principles of Food Processing and Engineering, 2nd edition*, Aspen Press, 1999) the identical descriptions and equations from materials science as relating to food products. The same basic understanding pervades both fields, namely that product performance (mechanical, chemical, environmental, nutritive, etc.) depends on structure, and that structure in turn depends on processing history. For most engineering materials this is limited to chemical composition and thermo-mechanical processing, but for food products it also includes genetics — breeding plants and animals to produce desirable structural properties.

In all cases, there is great interest in quantifying the various aspects of structure, and in many cases this involves imaging the structure and making measurements on the images. The images may be simple macroscopic or microscopic light images, including confocal light microscopy, but can also include electron images (with either the transmission or scanning electron microscope — SEM and TEM), atomic force microscope (AFM) images of surfaces, magnetic resonance (MRI) or computed tomography (CT) images of internal structure, and many more. Some techniques that we do not normally think of as imaging produce data sets that may be best interpreted as images, by plotting the data so that the eye (and the computer, with appropriate software) can identify trends, optima, etc. Even a simple one-dimensional graph such as a stress-strain curve may reveal more (e.g., the fractal irregularities of the curve) to the eye than the column of numbers from which it was plotted, and this becomes more significant for two-dimensional pictures (but unfortunately becomes more difficult for higher dimensionalities, because of the problems of plotting and viewing n-dimensional data).

In addition to teaching undergraduates about the basics of materials, I also taught a graduate course in image analysis and stereology. Although listed as a materials science course, this consistently attracted significant numbers of students from other majors, including textiles, wood and paper products, biology, the vet school, even archaeology — and a steady trickle of food science students. So eventually I was asked to sit on several graduate student advisory committees in the Food Science Department, got to know some of the faculty there, suggested various ways that image analysis could be used to measure structures of interest, and in the process got something of an education about food microstructure (and became more aware — not necessarily in a positive way — of what I was personally consuming).

That in turn led to contacts with other researchers, at other universities such as Penn State and the University of Guelph, to societies and organizations such as the Food Structure and Functionality Forum (a division of the AOCS), Agriculture and Agri-Food Canada, and the Hydrocolloids conferences, and to various corporations and their food interests, ranging from tiny (a specialty chocolate manufacturer and the producer of a nutraceutical supplement with microencapsulated omega-3 fatty acids) to large (major producers of cake mixes, baked goods, processed meats, and so on). During this process, I have been continually surprised to see the same questions and problems surfacing over and over. While the food products themselves, and to some extent the images and terminology, differ widely, the structural properties of interest, and the appropriate ways to determine them from images, tend to be much the same.

That gives me hope that this book can usefully summarize the basic procedures that will be useful to many of these researchers. The topics covered are the acquisition and processing of the images, the measurement of appropriate microstructural parameters, and the interpretation of those numbers required by the fact that the structures are generally three-dimensional while the images are usually two-dimensional. In most general textbooks in image analysis, including my own (*The Image Processing Handbook, 4th edition*, CRC Press, 2002), the organization typically begins with the characteristics of cameras, proceeds through the various processing steps on color or grey scale images, and then discusses segmentation or thresholding and the processing and measurement of binary images. The data from these measurements is then used as the subject for statistical analysis and perhaps the construction of expert systems for feature recognition.

As a framework for instruction, that sequential organization is useful, but for this text I am risking a different approach. This book starts with basic stereology, which is the essentially geometric science that relates three-dimensional structures to the measurements that can be made on two-dimensional slices such as typical microscope images. From this consideration emerges the fundamental ideas of what *can* and *should* be measured on structures, and that will guide subsequent chapters of the book. It is conventional to think about measurement as the last step, after processing and thresholding. But in complex structures it is often very useful to obtain measurement data directly from the processing operations themselves. Consequently, measurements will be introduced throughout the various chapters. The reader is invited to relate these measurements to the important history-structure-function relationships in the particular kinds of food products of personal interest.

Also, processing of images in the “pixel” or spatial domain is often considered separately from processing in the frequency or Fourier domain, because the math appears rather different. Since the math is largely suppressed in this book anyway (which emphasizes the underlying concepts and concentrates on the visual interpretation of the results), I have decided to avoid that separation and mix both approaches together. The resulting organization is based on what I have found to be a useful step-by-step approach to extraction of information from images, largely driven by what information is being sought.

This book does not contain the usual hundreds of literature citations for the various procedures described. The presentation here does not pretend to include the technical details of the various algorithms and procedures, just illustrations of how they are used. There are plenty of texts, my own included, that do have those references, as well as fuller explanations of the underlying math and programs. For anyone planning to write their own programs, reference to those texts will be necessary anyway and will lead directly to the primary sources. The intent here is to familiarize the food scientist with ways of thinking about images, their processing and measurement. To borrow a description one of my students once used, it is about playing music, not writing it.

Also, there is no list of citations to work that has used these methods to measure food structures. My rationale for this absence is that I am involved with the measurement process and not the food science, and am reluctant to judge which papers are meaningful and which are not. It is my impression that there has been some very good work done from a measurement standpoint (as well as much that is questionable), but whether that translates to a better understanding of the processing and properties of the food structures is beyond my range of understanding, in spite of the best efforts of some folks acknowledged below to educate me.

Finally, a word of caution to the reader: This is not something you can really learn by reading through the book and thinking about it — you need to do it yourself. To continue the analogy from above, you have to play the music, not just listen to it. Learning from words and pictures in a book is no substitute for learning by trying out the methods on real images and seeing the results of step-by-step procedures. It helps to have your own images of the structures of particular interest. And, of course, that means you need the appropriate cameras, computers, software and so on. Most of the techniques described in the book can be performed using a wide variety of commercially available software, ranging from expensive dedicated image processing and analysis packages such as Media Cybernetics’ Image Pro Plus or Universal Imaging’s Metamorph programs, to data handling environments such as Matlab which can also handle images.

That is not intended as an endorsement and is certainly not a comprehensive list — there are literally hundreds of companies who sell image processing or analysis software, some highly specialized for particular niche markets. Each program will impose some limitations on what you can accomplish but more importantly will typically use quite different terminology to describe the operations, and will have the functions organized in entirely different ways. Learning the basics of what you can do and want to do from this book is only the first step; then you have to study the software manual to find out how to do it.

As an aid to the researcher who does not already have software in place, or who finds that their particular package lacks some of the tools described here, I have collaborated with Reindeer Graphics, Inc. (<http://www.ReindeerGraphics.com>), a company run by my son and by one of my former students, to produce a set of Photoshop®-compatible plugins that implement each of the algorithms used in the text. Information on the software is available online; the CD that installs the software includes a lengthy tutorial showing how to use the various procedures, with a large suite of test images for instructional purposes (the software can also be used with any other images). There are two packages: Fovea Pro and The Image Processing Tool Kit. The Tool Kit is intended as a low-cost educational package, limited to 8 bit per channel grey scale and 24 bit RGB color images, adequate for bright field microscopy and most SEM images. Fovea Pro includes all of the Tool Kit functions and also works with 16 bit per channel images (important for dark field and fluorescence images, transmission EM pictures, and most surface imaging data) including 48 bit RGB color (such as the output from most film or flatbed scanners).

Isolating each function as a separate menu item facilitates learning what each method does, but the software is not limited to teaching. It can also be used for real analysis, and sequences of operations can easily be created (e.g., using Photoshop® Actions) to carry out complicated automatic analysis of batches of images. Adobe Photoshop was selected as a platform for this because it is relatively inexpensive, well documented and with a reasonable learning curve, and already in widespread use in labs for image acquisition, presentation, annotation, etc. Photoshop supports a wide variety of image formats and acquisition devices (scanners, cameras, etc.). Also, the fact that Photoshop is so widely used means that other programs have adopted the same convention for add-on plugins, and Photoshop-compatible plugins can also be used by many other programs on both Windows and Macintosh computers, ranging from inexpensive software such as Jasc's Paint Shop Pro to costly professional software such as Media Cybernetics' Image Pro Plus.

My special thanks go out to the many food scientists who have contributed generously to this book. Their support has ranged from general encouragement for the idea that it was time that such a text was available, to taking the time to educate me about a particular food product or problem, to providing example images. I can not begin to list here everyone who has helped, but I have tried to credit each picture supplied by someone else in the captions (and I apologize if I have missed someone unintentionally due to my own poor record keeping!). Special thanks are due to Allen Foegeding at North Carolina State University for getting this whole project started, reviewing the text to try to keep me from saying nonsensical things about food, and helping a lot along the way; to José Aguilera and David Stanley for writing their book and encouraging mine; to Alex Marangoni, Howard Swatland and others at the University of Guelph for sharing their library of many years of images; to Ken Baker for providing access to his image collection; and to Greg Ziegler at Penn State University and Paula Allan-Wojtas at Agriculture and Agri-Food Canada, for images, ideas, and invitations.

John Russ
Raleigh, NC

1 Stereology

THE NEED FOR STEREOLOGY

Before starting with the process of acquiring, correcting and measuring images, it seems important to spend a chapter addressing the important question of just what it is that can and should be measured, and what cannot or should not be. The temptation to just measure everything that software can report, and hope that a good statistics program can extract some meaningful parameters, is both naïve and dangerous. No statistics program can correct, for instance, for the unknown but potentially large bias that results from an inappropriate sampling procedure.

Most of the problems with image measurement arise because of the nature of the sample, even if the image itself captures the details present perfectly. Some aspects of sampling, while vitally important, will not be discussed here. The need to obtain a representative, uniform, randomized sample of the population of things to be measured should be obvious, although it may be overlooked, or a procedure used that does not guarantee an unbiased result. A procedure, described below, known as systematic random sampling is the most efficient way to accomplish this goal once all of the contributing factors in the measurement procedure have been identified.

In some cases the images we acquire are of 3D objects, such as a dispersion of starch granules or rice grains for size measurement. These pictures may be taken with a macro camera or an SEM, depending on the magnification required, and provided that some care is taken in dispersing the particles on a contrasting surface so that small particles do not hide behind large ones, there should be no difficulty in interpreting the results. Bias in assessing size and shape can be introduced if the particles lie down on the surface due to gravity or electrostatic effects, but often this is useful (for example, measuring the length of the rice grains).

Much of the interest in food structure has to do with internal microstructure, and that is typically revealed by a sectioning procedure. In rare instances volume imaging is performed, for instance, with MRI or CT (magnetic resonance imaging and computerized tomography), both techniques borrowed from medical imaging. However, the cost of such procedures and the difficulty in analyzing the resulting data sets limits their usefulness. Full three-dimensional image sets are also obtained from either optical or serial sectioning of specimens. The rapid spread of confocal light microscopes in particular has facilitated capturing such sets of data. For a variety of reasons — resolution that varies with position and direction, the large size of the data files, and the fact that most 3D software is more concerned with rendering visual displays of the structure than with measurement — these volume imaging results are not commonly used for structural measurement.

Most of the microstructural parameters that robustly describe 3D structure are more efficiently determined using stereological rules with measurements performed

on section images. These may be captured from transmission light or electron microscopes using thin sections, or from light microscopes using reflected light, scanning electron microscopes, and atomic force microscopes (among others) using planar surfaces through the structure. For measurements on these images to correctly represent the 3D structure, we must meet several criteria. One is that the surfaces are properly representative of the structure, which is sometimes a non-trivial issue and is discussed below. Another is that the relationships between two and three dimensions are understood.

That is where stereology (literally the study of three dimensions, and unrelated to stereoscopy which is the viewing of three dimensions using two eye views) comes in. It is a mathematical science developed over the past four decades but with roots going back two centuries. Deriving the relationships of geometric probability is a specialized field occupied by a few mathematicians, but using them is typically very simple, with no threatening math. The hard part is to understand and visualize the meaning of the relationships and recognizing the need to use them, because they tell us what to measure and how to do it. The rules work at all scales from nm to light-years and are applied in many diverse fields, ranging from materials science to astronomy.

Consider for example a box containing fruit — melons, grapefruit and plums — as shown in Figure 1.1. If a section is cut through the box and intersects the fruit, then an image of that section plane will show circles of various colors (green, yellow and purple, respectively) that identify the individual pieces of fruit. But the sizes of the circles are not the sizes of the fruit. Few of the cuts will pass through the equator of a spherical fruit to produce a circle whose diameter would give the size of the sphere. Most of the cuts will be smaller, and some may be very small where the plane of the cut is near the north or south pole of the sphere. So measuring the 3D sizes of the fruit is not possible directly.

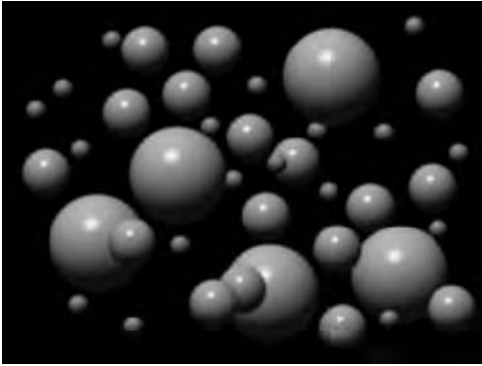
What about the number of fruits? Since they have unique colors, does counting the number of intersections reveal the relative abundance of each type? No. Any plane cut through the box is much more likely to hit a large melon than a small plum. The smaller fruits are under-represented on the plane. In fact, the probability of intersecting a fruit is directly proportional to the diameter. So just counting doesn't give the desired information, either.

Counting the features present can be useful, if we have some independent way to determine the mean size of the spheres. For example, if we've already measured the sizes of melons, plums and grapefruit, then the number per unit volume N_V of each type fruit in the box is related to the number of intersections per unit area N_A seen on the 2D image by the relationship

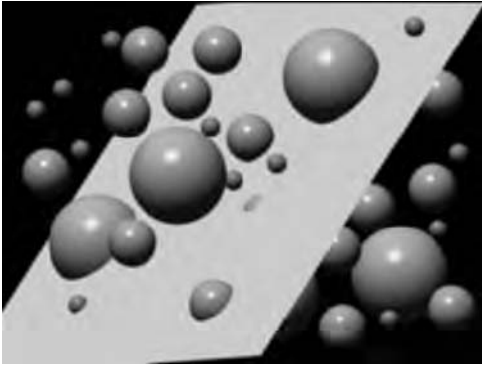
$$N_V = \frac{N_A}{D_{mean}} \quad (1.1)$$

where D_{mean} is the mean diameter.

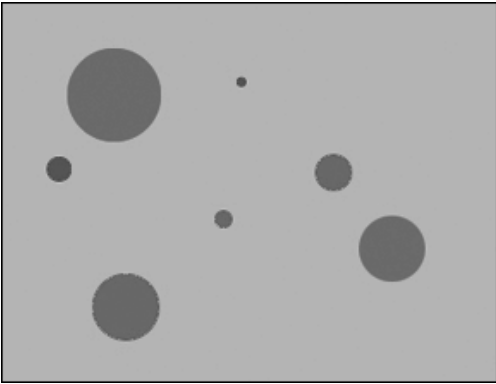
In stereology the capital letter N is used for number and the subscript V for volume and A for area, so this would be read as “Number per unit volume equals



(a)



(b)



(c)

FIGURE 1.1 (See color insert following page 150.) Schematic diagram of a box containing fruit: (a) green melons, yellow grapefruit, purple plums; (b) an arbitrary section plane through the box and its contents; (c) the image of that section plane showing intersections with the fruit.

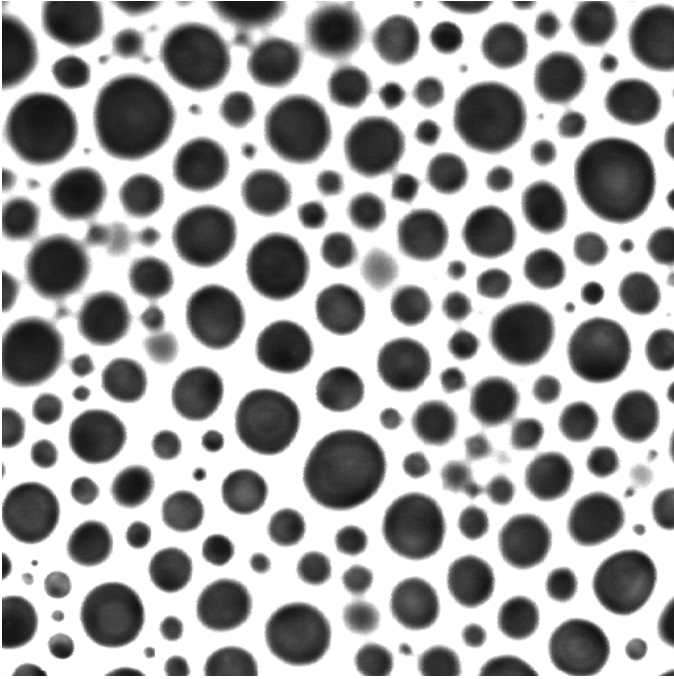


FIGURE 1.2 Section image through a foamed food product. (Courtesy of Allen Foegeding, North Carolina State University, Department of Food Science)

number per unit area divided by mean diameter.” Rather than using the word “equals” it would be better to say “is estimated by” because most of the stereological relationships are statistical in nature and the measurement procedure and calculation give a result that (like all measurement procedures) give an estimate of the true result, and usually a way to also determine the precision of the estimate.

The formal relationship shown in Equation 1.1 relates the expected value (the average of many observed results) of the number of features per unit area to the actual number per unit volume times the mean diameter. For a series of observations (examination of multiple fields of view) the average result will approach the expected value, subject to the need for examining a representative set of samples while avoiding any bias. Most of the stereological relationships that will be shown are for expected values.

Consider a sample like the thick-walled foam in Figure 1.2 (a section through a foamed food product). The size of the bubbles is determined by the gas pressure, liquid viscosity, and the size of the hole in the nozzle of the spray can. If this mean diameter is known, then the number of bubbles per cubic centimeter can be calculated from the number of features per unit area using Equation 1.1. The two obvious things to do on an image like those in Figures 1.1 and 1.2 are to count features and measure the sizes of the circles, but both require stereological interpretation to yield a meaningful result.

This problem was recognized long ago, and solutions have been proposed since the 1920s. The basic approach to recovering the size distribution of 3D features from the image of 2D intersections is called “unfolding.” It is now out of favor with most stereologists because of two important problems, discussed below, but since it is still useful in some situations (and is still used in more applications than it probably should be), and because it illustrates an important way of thinking about three dimensions, a few paragraphs will be devoted to it.

UNFOLDING SIZE DISTRIBUTIONS

Random intersections through a sphere of known radius produce a distribution of circle sizes that can be calculated analytically as shown in Figure 1.3. If a large number of section images are measured, and a size distribution of the observed circles is determined, then the very largest circles can only have come from near-equatorial cuts through the largest spheres. So the size of the largest spheres is established, and their number can be calculated using Equation 1.1.

But if this number of large spheres is present, the expected number of cross sections of various different smaller diameters can be calculated using the derived relationship, and the corresponding number of circles subtracted from each smaller bin in the measured size distribution. If that process leaves a number of circles remaining in the next smallest size bin, it can be assumed that they must represent near-equatorial cuts through spheres of that size, and their number can be calculated. This procedure can be repeated for each of the smaller size categories, typically 10 to 15 size classes. Note that this does not allow any inference about the size sphere that corresponds to any particular circle, but is a statistical relationship that depends upon the collective result from a large number of intersections.

If performed in this way, a minor problem arises. Because of counting statistics, the number of circles in each size class has a finite precision. Subtracting one number

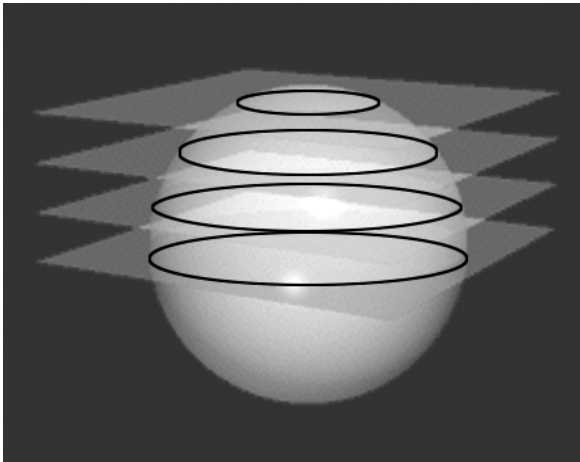


FIGURE 1.3 Schematic diagram of sectioning a sphere to produce circles of different sizes.

(the expected number of circles based on the result in a larger class) from another (the number of circles observed in the current size class) leaves a much smaller net result, but with a much larger statistical uncertainty. The result of the stepwise approach leads to very large statistical errors accumulating for the smallest size classes.

That problem is easily solved by using a set of simultaneous equations and solving for all of the bins in the distribution at the same time. Tables of coefficients that calculate the number of spheres in each size class (i) from the number of circles in size class (j) have been published many times, with some difference depending on how the bin classes are set up. One widely used version is shown in Table 1.1. The mathematics of the calculation is very simple and easily implemented in a spreadsheet. The number of spheres in size class i is calculated as the sum of the number of circles in each size class j times an alpha coefficient (Equation 1.2). Note that half of the matrix of alpha values is empty because no large circles can be produced by small spheres.

$$N_{V_i} = \sum_j \alpha_{ij} \cdot N_{A_j} \quad (1.2)$$

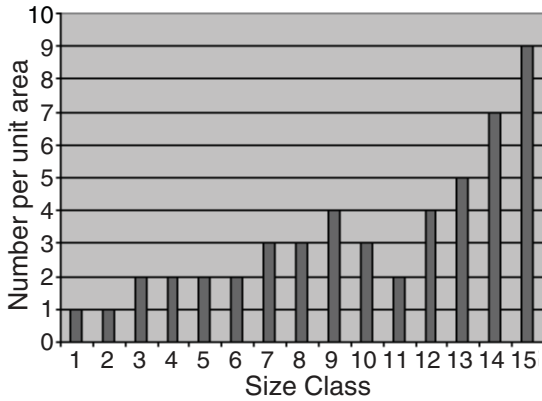
Figure 1.4 shows the application of this technique to the bubbles in the image of Figure 1.2. The circle size distribution shows a wide variation in the sizes of the intersections of the bubbles with the section plane, but the calculated sphere size distribution shows that the bubbles are actually all of the same size, within counting statistics. Notice that this calculation does not directly depend on the actual sizes of the features, but just requires that the size classes represent equal-sized linear increments starting from zero.

Even with the matrix solution of all equations at the same time, this is still an ill conditioned problem mathematically. That means that because of the subtractions (note that most of the alpha coefficients are negative, carrying out the removal of smaller circles expected to correspond to larger spheres) the statistical precision of the resulting distribution of sphere sizes is much larger (worse) than the counting precision of the distribution of circle sizes. Many stereological relationships can be estimated satisfactorily from only a few images and a small number of counts. However, unfolding a size distribution does not fit into this category and very large numbers of raw measurements are required.

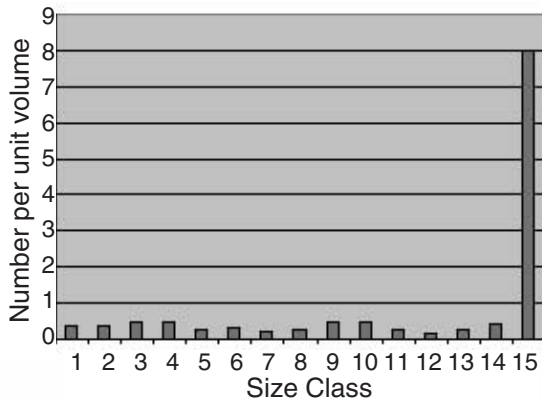
The more important problem, which has led to the attempts to find other techniques for determining 3D feature sizes, is that of shape. The alpha matrix values depend critically on the assumption that the features are all spheres. If they are not, the distribution of sizes of random intersections changes dramatically. As a simple example, cubic particles produce a very large number of small intersections (where a corner is cut) and the most probable size is close to the area of a face of the cube, not the maximum value that occurs when the cube is cut diagonally (a rare event). For the sphere, on the other hand, the most probable value is large, close to the equatorial diameter, and very small cuts that nip the poles of the sphere are rare, as shown in Figure 1.5.

TABLE 1.1
Matrix of Alpha Values Used to Convert the Distribution of Number of Circles per Unit Area
to Number of Spheres per Unit Volume

| $N_A(1)$ | $N_A(2)$ | $N_A(3)$ | $N_A(4)$ | $N_A(5)$ | $N_A(6)$ | $N_A(7)$ | $N_A(8)$ | $N_A(9)$ | $N_A(10)$ | $N_A(11)$ | $N_A(12)$ | $N_A(13)$ | $N_A(14)$ | $N_A(15)$ |
|----------|----------|----------|----------|----------|----------|----------|----------|----------|-----------|-----------|-----------|-----------|-----------|-----------|
| 0.26491 | -0.19269 | 0.01015 | -0.01636 | -0.00538 | -0.00481 | -0.00327 | -0.00250 | -0.00189 | -0.00145 | -0.00109 | -0.00080 | -0.00055 | -0.00033 | -0.00013 |
| | 0.27472 | -0.19973 | 0.01067 | -0.01691 | -0.00549 | -0.00491 | -0.00330 | -0.00250 | -0.00186 | -0.00139 | -0.00101 | -0.00069 | -0.00040 | -0.00016 |
| | | 0.28571 | -0.20761 | 0.01128 | -0.01751 | -0.00560 | -0.00501 | -0.00332 | -0.00248 | -0.00180 | -0.0012 | -0.00087 | -0.00051 | -0.00020 |
| | | | 0.29814 | -0.21649 | 0.01200 | -0.01818 | -0.00571 | -0.00509 | -0.00332 | -0.00242 | -0.00169 | -0.00113 | -0.00066 | -0.00026 |
| | | | | 0.31235 | -0.22663 | 0.01287 | -0.01893 | -0.00579 | -0.00516 | -0.00327 | -0.00230 | -0.00150 | -0.00087 | -0.00034 |
| | | | | | 0.32880 | -0.23834 | 0.01393 | -0.01977 | -0.00584 | -0.00518 | -0.00315 | -0.00208 | -0.00117 | -0.00045 |
| | | | | | | 0.34816 | -0.25208 | 0.01527 | -0.02071 | -0.00582 | -0.00512 | -0.00288 | -0.00167 | -0.00062 |
| | | | | | | | 0.37139 | -0.26850 | 0.01704 | -0.02176 | -0.00565 | -0.00488 | -0.00234 | -0.00094 |
| | | | | | | | | 0.40000 | -0.28863 | 0.01947 | -0.02293 | -0.00516 | -0.00427 | -0.00126 |
| | | | | | | | | | 0.43644 | -0.31409 | 0.02308 | -0.02416 | -0.00393 | -0.00298 |
| | | | | | | | | | | 0.48507 | -0.34778 | 0.02903 | -0.02528 | -0.00048 |
| | | | | | | | | | | | 0.55470 | -0.39550 | 0.04087 | -0.02799 |
| | | | | | | | | | | | | 0.66667 | -0.47183 | 0.08217 |
| | | | | | | | | | | | | | 0.89443 | -0.68328 |
| | | | | | | | | | | | | | | 1.00000 |



(a)



(b)

FIGURE 1.4 Calculation of sphere sizes: (a) measured circle size distribution from Figure 1. 2; (b) distribution of sphere sizes calculated from a using Equation 1.2 and Table 1.1. The plots show the relative number of objects as a function of size class.

In theory it is possible to compute an alpha matrix for any shape, and copious tables have been published for a wide variety of polygonal, cylindrical, ellipsoidal, and other geometric shapes. But the assumption still applies that all of the 3D features present have the same shape, and that it is known. Unfortunately, in real systems this is rarely the case (see the example of the pores, or “cells” in the bread in Figure 1.6). It is very common to find that shapes vary a great deal, and often vary systematically with size. Such variations invalidate the fundamental approach of size unfolding.

That the unfolding technique is still in use is due primarily to two factors: first, there really are some systems in which a sphere is a reasonable model for feature shape. These include liquid drops, for instance in an emulsion, in which surface tension produces a spherical shape. Figure 1.7 shows spherical fat droplets in

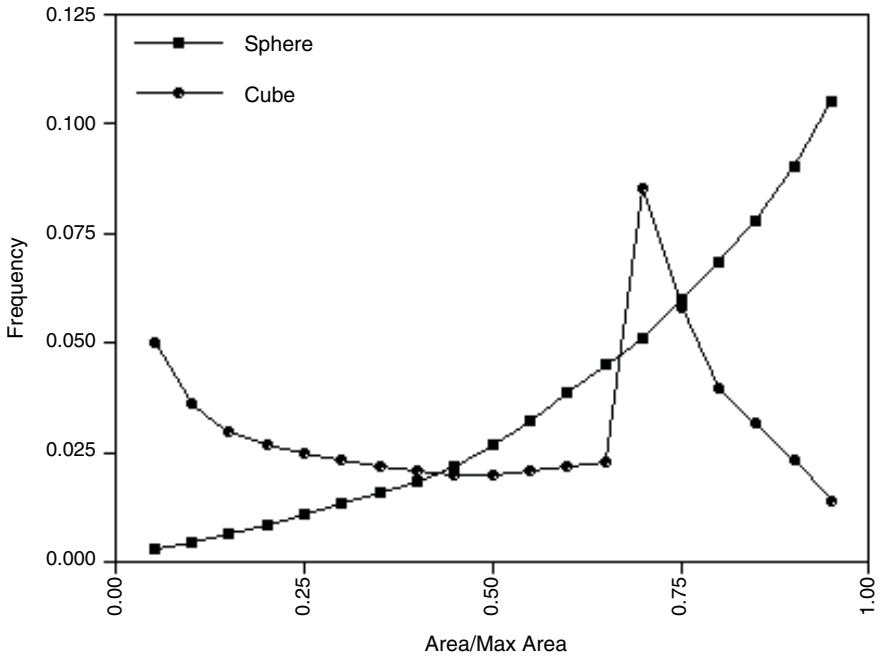


FIGURE 1.5 Probability distributions for sections through a sphere compared to a cube.

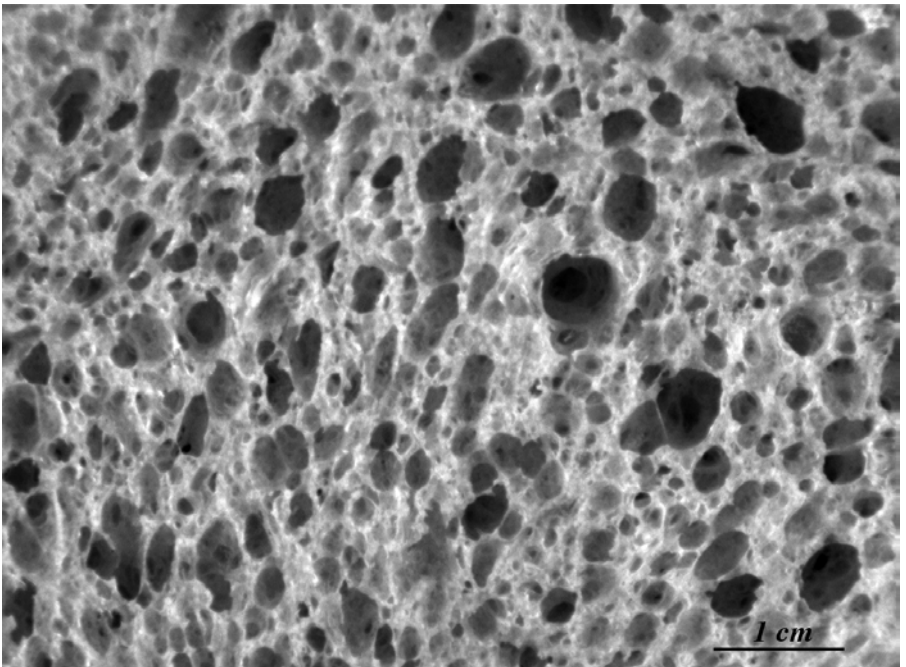
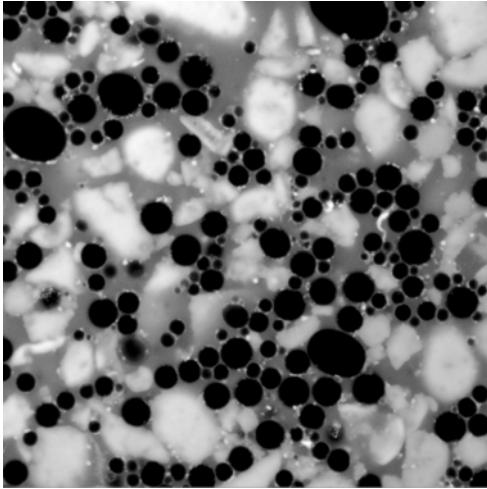
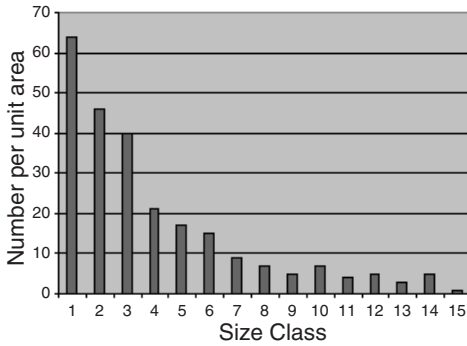


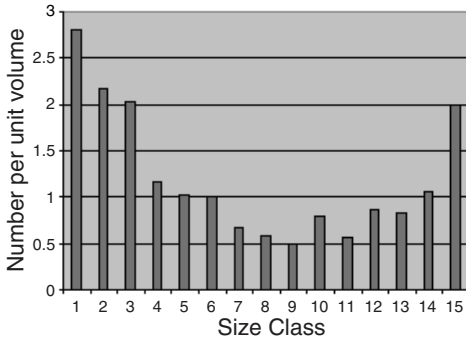
FIGURE 1.6 Image of pores in a bread slice showing variations in shape and size. (Courtesy of Diana Kittleson, General Mills)



(a)



(b)



(c)

FIGURE 1.7 Calculation of sphere size distribution: (a) image of fat droplets in mayonnaise (Courtesy of Anke Janssen, ATO B.V., Food Structure and Technology); (b) measured histogram of circle sizes; (c) calculated distribution of sphere sizes. The plots show the relative number of objects as a function of size class.

mayonnaise, for which the circle size distribution can be processed to yield a distribution of sphere sizes. Note that some of the steps needed to isolate the circles for measurement will be described in detail in later chapters.

The second reason for the continued use of sphere unfolding is ignorance, laziness and blind faith. The notion that “maybe the shapes aren’t really spheres, but surely I can still get a result that will compare product A to product B” is utterly wrong (different shapes are likely to bias the results in quite unexpected ways). But until researchers gain familiarity with some of the newer techniques that permit unbiased measurement of the size of three-dimensional objects they are reluctant to abandon the older method, even if deep-down they know it is not right.

Fortunately there are methods, such as the point-sampled intercept and disector techniques described below, that allow the unbiased determination of three-dimensional sizes regardless of shape. Many of these methods are part of the so-called “new stereology,” “design-based stereology,” or “second-order stereology” that have been developed within the past two decades and are now becoming more widely known. First, however, it will be useful to visit some of the “old” stereology, classical techniques that provide some very important measures of three-dimensional structure.

VOLUME FRACTION

Going back to the structure in Figure 1.2, if the sphere size is known, the number can be calculated from the volume fraction of bubbles, which can also be measured from the 2D image. In fact, determining volume fraction is one of the most basic stereological procedures, and one of the oldest. A French geologist interested in determining the volume fraction of ore in rock 150 years ago, realized that the area fraction of a section image that showed the ore gave the desired result. The stereologists’ notation represents this as Equation 1.3, in which the V_V represents the volume of the phase or structure of interest per unit volume of sample, and the A_A represents the area of that phase or structure that is visible in the area of the image. As noted before, this is an expected value relationship that actually says the expected value of the area fraction observed will converge to the volume fraction.

$$V_V = A_A \quad (1.3)$$

To understand this simple relationship, imagine the section plane sweeping through a volume; the area of the intersections with the ore integrates to the total volume of ore, and the area fraction integrates to the volume fraction. So subject to the usual caveats about requiring representative, unbiased sampling, the expected value of the area fraction is (or measures) the volume fraction.

In the middle of the nineteenth century, the area fraction was not determined with digital cameras and computers, of course; not even with traditional photography, which had only just been invented and was not yet commonly performed with microscopes. Instead, the image was projected onto a piece of paper, the features of interest carefully traced, and then the paper cut and weighed. The equivalent

modern measurement of area fraction can often be accomplished by counting pixels in the image histogram, as shown in Figure 1.8. The histogram is simply a plot of the number of pixels having each of the various brightness levels in the image, often 256. The interpretation of the histogram will be described in subsequent chapters. Although very efficient, this is not always the preferred method for measurement of volume fraction, because the precision of the measurement is better estimated using other approaches.

The measurement of the area represented by peaks in the histogram is further complicated by the fact that not all of the pixels in the image have brightness values that place them in the peaks. As shown in Figure 1.9, there is generally a background level between the peaks that can represent a significant percentage of the total image area. In part this is due to the finite area of each pixel, which averages the information from a small square on the image. Also, there is usually some variation in pixel brightness (referred to generally as noise) even from a perfectly uniform area. Chapter 3 discusses techniques for reducing this noise. Notice that this image is not a photograph of a section, but has been produced non-destructively by X-ray tomography. The brightness is a measure of local density.

The next evolution in methodology for measuring volume fraction came fifty years after the area fraction technique, again introduced as a way to measure minerals. Instead of measuring areas, which is difficult, a random line was drawn on the image and the length of that line which passed through the structure of interest was measured (Figure 1.10). The line length fraction is also an estimate of the volume fraction. For understanding, imagine the line sweeping across the image; the line length fraction integrates to the area fraction. The stereological notation is shown in Equation 1.4, where L_L represents the length of the intersections as a fraction of the total line length.

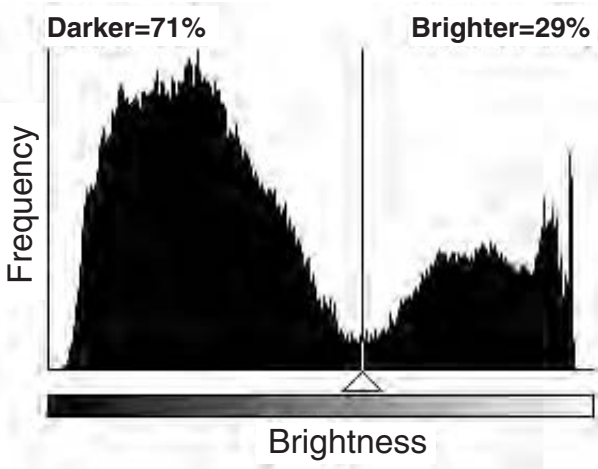
$$V_V = L_L \quad (1.4)$$

The advantage of this method lies in the greater ease with which the line length can be measured as compared to area measurements. Even in the 1950s my initial experience with measurement of volume fraction used this approach. A small motor was used to drive the horizontal position of a microscope stage, with a counter keeping track of the total distance traveled. Another counter could be engaged by pressing a key, which the human observer did whenever the structure of interest was passing underneath the microscope's crosshairs. The ratio of the two counter numbers gave the line length fraction, and hence the volume fraction. Replacing the human eye with an electronic sensor whose output could be measured to identify the phase created an automatic image analyzer.

By the middle of the twentieth century, a Russian metallurgist had developed an even simpler method for determining volume fraction that avoided the need to make a measurement of area or length, and instead used a counting procedure. Placing a grid of points on the image of the specimen (Figure 1.11), and counting the fraction of them that fall onto the structure of interest, gives the point fraction

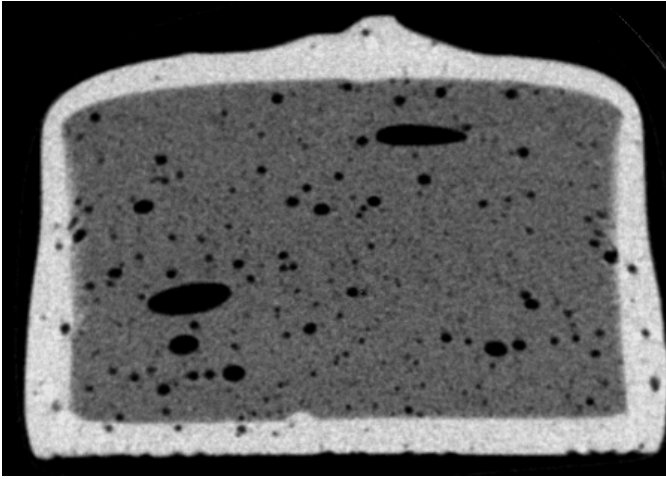


(a)

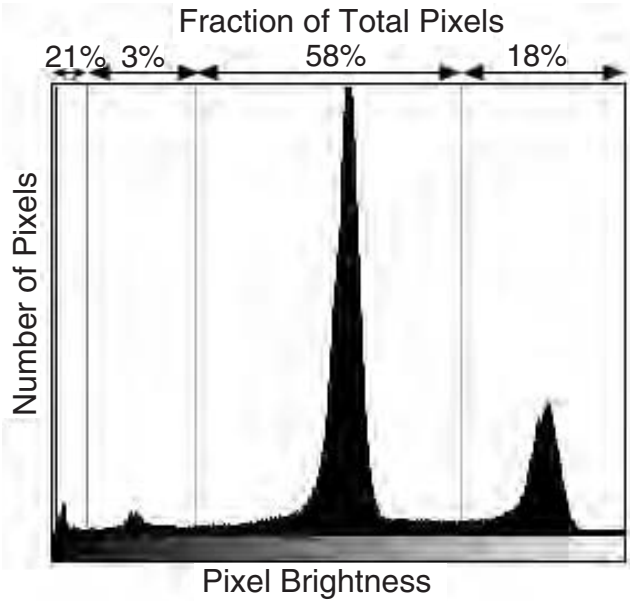


(b)

FIGURE 1.8 Using the histogram to measure area fraction: (a) photograph of a beef roast, after some image processing to enhance visibility of the fat and bones; (b) histogram of just the portion of the image containing the roast. The plot shows the number of pixels with each possible shade of brightness; the threshold setting shown (vertical line) separates the dark meat from the lighter fat and bone shows that 71% of the roast (by volume) is meat. The histogram method does not provide any information about the spatial distribution of the fat (marbling, etc.), which will be discussed in Chapter 4.



(a)



(b)

FIGURE 1.9 X-ray tomographic section through a Three Musketeers candy bar with its brightness histogram. The peaks in the histogram correspond to the holes, interior and coating seen in the image, and can be used to measure their volume fraction. (Courtesy of Greg Ziegler, Penn State University Food Science Department)

P_p (Equation 1.5), which is also a measure of the volume fraction. It is easy to see that as more and more points are placed in the 3D volume of the sample, that the point fraction must become the volume fraction.

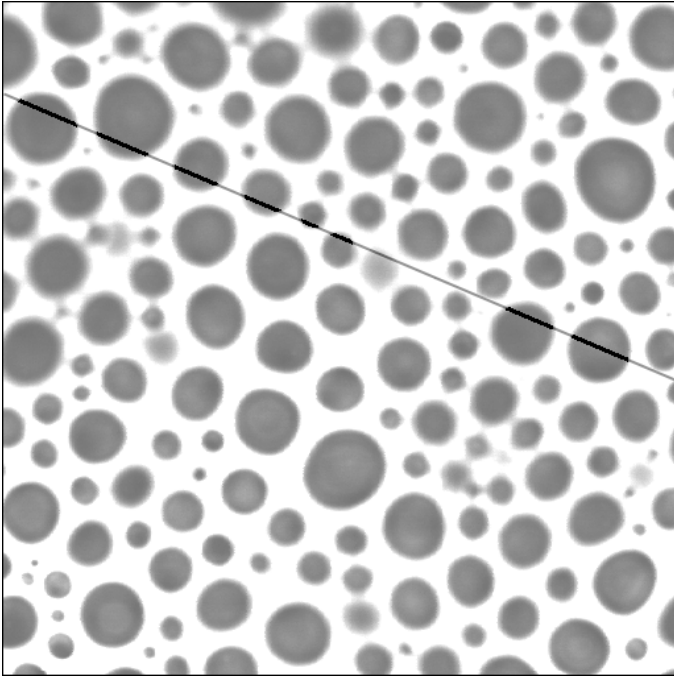


FIGURE 1.10 The image from Figure 1.2 with a random line superimposed. The sections that intersect pores are highlighted. The length of the highlighted sections divided by the length of the line estimates the volume fraction.

$$V_v = P_p \tag{1.5}$$

The great advantage of a counting procedure over a measurement operation is not just that it is easier to make, but that the precision of the measurement can be predicted directly. If the sampled points are far enough apart that they act as independent probes into the volume (which in practice means that they are far enough apart then only rarely will two grid points fall onto the same portion of the structure being measured), then the counting process obeys Poisson statistics and the standard deviation in the result is simply the square root of the number of events counted.

In the grid procedure the events counted are the cases in which a grid point lies on structure being measured. So as an example, if a 49 point grid (7×7 array of points) is superimposed on the image in Figure 1.11, 16 of the points fall onto the bubbles. That estimates the volume fraction as $16/49 = 33\%$. The square root of 16 is 4, and $4/16$ is 25%, so that is the estimate of the relative accuracy of the measurement (in other words, the volume fraction is reported as 0.33 ± 0.08). In order to achieve a measurement precision of 10%, it would be necessary to look at additional fields of view until 100 counts (square root = 10; $10/100 = 10\%$) had been accumulated. Based on observing 16 counts on this image, we would anticipate needing a total of 6 fields of view to reach that level of precision. For 5%, 400 counts are needed, and so forth.

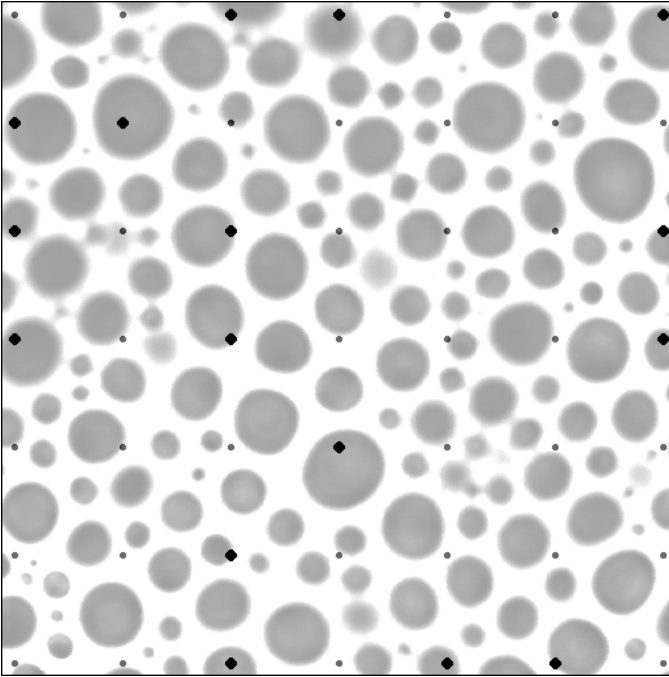


FIGURE 1.11 The image from Figure 1.2 with a 49 point (7×7) grid superimposed (points are enlarged for visibility). The points that lie on pores are highlighted. The fraction of the points that lie on pores estimates their volume fraction.

A somewhat greater number of points in the measurement grid would produce more hits. For example, using a 10×10 array of points on Figure 1.2 gives 33 hits, producing the same estimate of 33% for the volume fraction but with a 17% relative error rather than 25%. But the danger in increasing the number of grid points is that they may no longer be independent probes of the microstructure. A 10×10 grid comes quite close to the same dimension as the typical size and spacing of the bubbles. The preferred strategy is to use a rather sparse grid of points and to look at more fields of view. That assures the ability to use the simple prediction of counting statistics to estimate the precision, and it also forces looking at more microstructure so that a more representative sample of the whole object is obtained.

Another advantage of using a very sparse grid is that it facilitates manual counting. While it is possible to use a computer to acquire images, process and threshold them to delineate the structure of interest, generate a grid and combine it logically with the structure, and count the points that hit (as will be shown in Chapter 4), it is also common to determine volume fractions manually. With a simple grid having a small number of points (usually defined as the corners and intersections in a grid of lines, as shown in Figure 1.12), a human observer can count the number of hits at a glance, record the number and advance to another field of view.

At one time this was principally done by placing the grid on a reticle in the microscope eyepiece. With the increasing use of video cameras and monitors the

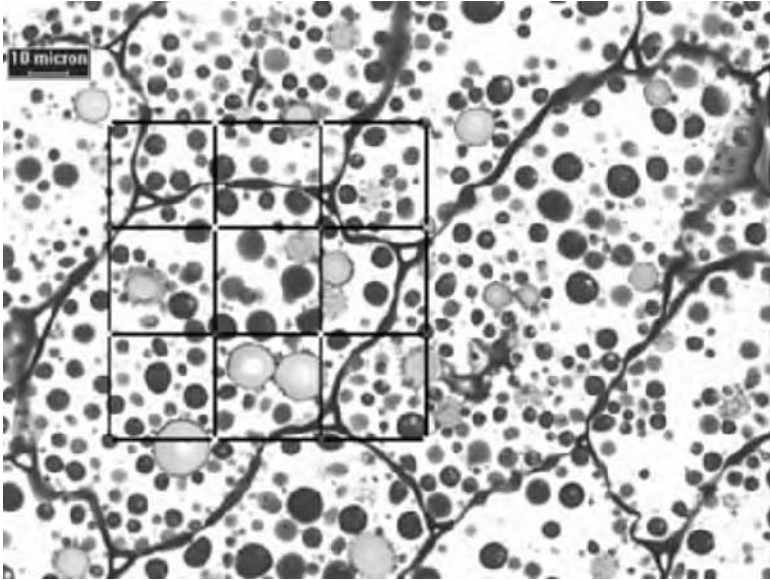


FIGURE 1.12 (See color insert following page 150.) A sixteen-point reticle randomly placed on an image of peanut cells stained with toluidine blue to show protein bodies (round, light blue) and starch granules (dark blue). The gaps at the junctions of the lines define the grid points and allow the underlying structure to be seen. Seven of the sixteen grid points lie on the starch granules (44%). The lines themselves are used to determine surface area per unit volume as described below (at the magnification shown, each line is 66 μm long). (Courtesy of David Pechak, Kraft Foods Technology Center)

same result can be achieved by placing the grid on the display monitor. Of course, with image capture the grid can be generated and superimposed by the computer. Alternately, printing grids on transparent acetate overlays and placing them on photographic prints is an equivalent operation.

By counting grid points on a few fields of view, a quick estimate of volume fraction can be obtained and, even if computer analysis of the images is performed subsequently to survey much more of the sample, at least a sufficiently good estimate of the final value is available to assist in the design of experiments, determination of the number of sections to cut and fields to image, and so on. This will be discussed a bit farther on. When a grid point appears to lie exactly on the edge of the structure, and it is not possible to confidently decide whether or not to count it, the convention is to count it as one-half.

This example of measuring volume fraction illustrates a trend present in many other stereological procedures. Rather than performing measurements of area or length, whenever possible the use of a grid and a counting operation is easier, and has a known precision that can be used to determine the amount of work that needs to be done to reach a desired overall result, for example to compare two or more types of material. Making measurements, either by hand or with a computer algorithm, introduces a finite source of measurement error that is often hard to estimate.

Even with the computer, some measurements, such as area and length, are typically more accurate than others (perimeter has historically been one of the more difficult things to measure well, as discussed in Chapter 5). Also, the precision depends on the nature of the sample and image. For example, measuring a few large areas or lengths produces much less total error than measuring a large number of small features. The counting approach eliminates this source of error, although of course it is still necessary to properly process and threshold the image so that the structure of interest is accurately delineated.

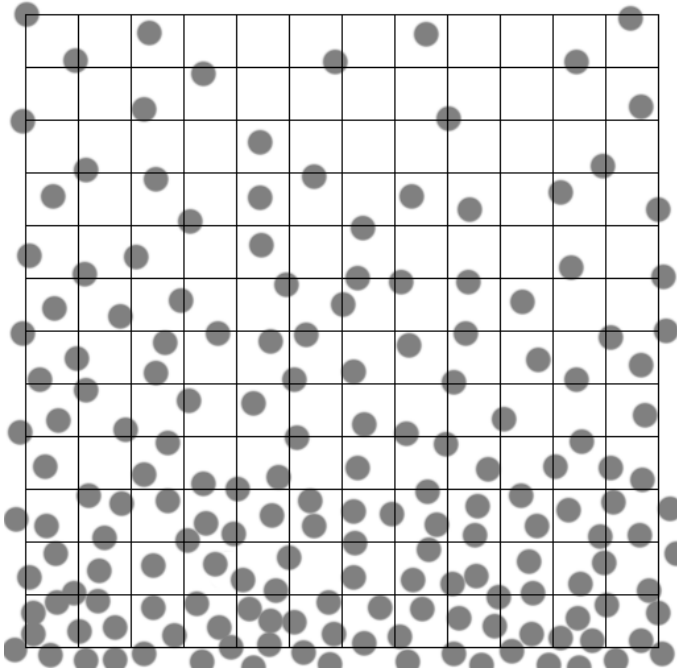
Volume fraction is an important property in most foods, since they are usually composed of multiple components. In addition to the total volume fraction estimated by uniform and unbiased (random) sampling, it is often important to study gradients in volume fraction, or to measure the individual volume of particular structures. These operations are performed in the same way, with just a few extra steps.

For example, sometimes it is practical to take samples that map the gradient to be studied. This could be specimens at the start, middle and end of a production run, or from the sides, top and bottom, and center of a product produced as a flat sheet, etc. Since each sample is small compared to the scale of the expected non-uniformities, each can be measured conventionally and the data plotted against position to reveal differences or gradients.

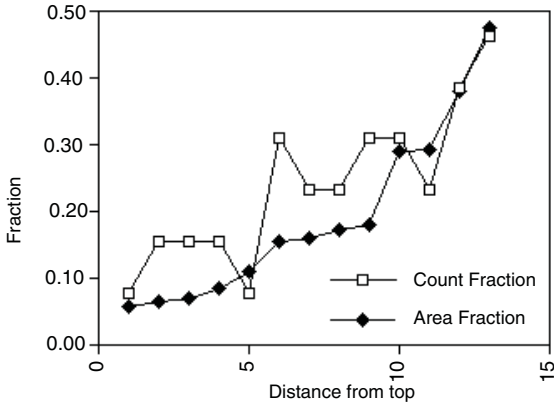
In other cases each image covers a dimension that encompasses the gradient. For instance, images of the cross section of a layer (Figure 1.13) may show a variation in the volume fraction of a phase from top to bottom. An example of such a simple vertical gradient could be the fat droplets settling by sedimentation in an oil and water emulsion such as full fat milk. Placing a grid of points on this image and recording the fraction of the number of points at each vertical position in the grid provides data to analyze the gradient, but since the precision depends on the number of hits, and this number is much smaller for each position, it is usually necessary to examine a fairly large number of representative fields to accumulate data adequate to show subtle trends.

Gradients can also sometimes be characterized by plotting the change of intensity or color along paths across images. This will be illustrated in Chapter 5. The most difficult aspect of most studies of gradients and nonuniformities is determining the geometry of the gradients so that an appropriate set of measurements can be made. For example, if the size of voids (cells) in a loaf of bread varies with distance from the outer crust, it is necessary to measure the size of each void and its position in terms of that distance. Fortunately, there are image processing tools (discussed in Chapter 4) that allow this type of measurement for arbitrarily shaped regions.

For a single object, the Cavalieri method allows measurement of total volume by a point count technique as shown in Figure 1.14. Ideally, a series of section images is acquired at regularly spaced intervals, and a grid of points placed on each one. Each point in the grid represents a volume, in the form of a prism whose area is defined by the spacing of the grid points and whose length is the spacing of the section planes. Counting the number of points that hit the structure and multiplying by the volume each one represents gives an estimate of the total volume.



(a)



(b)

FIGURE 1.13 Diagram of a simple vertical gradient with a superimposed grid. Counting the fraction of the grid points (b) measures the variation with position, but plotting the area fraction provides a superior representation from one image.

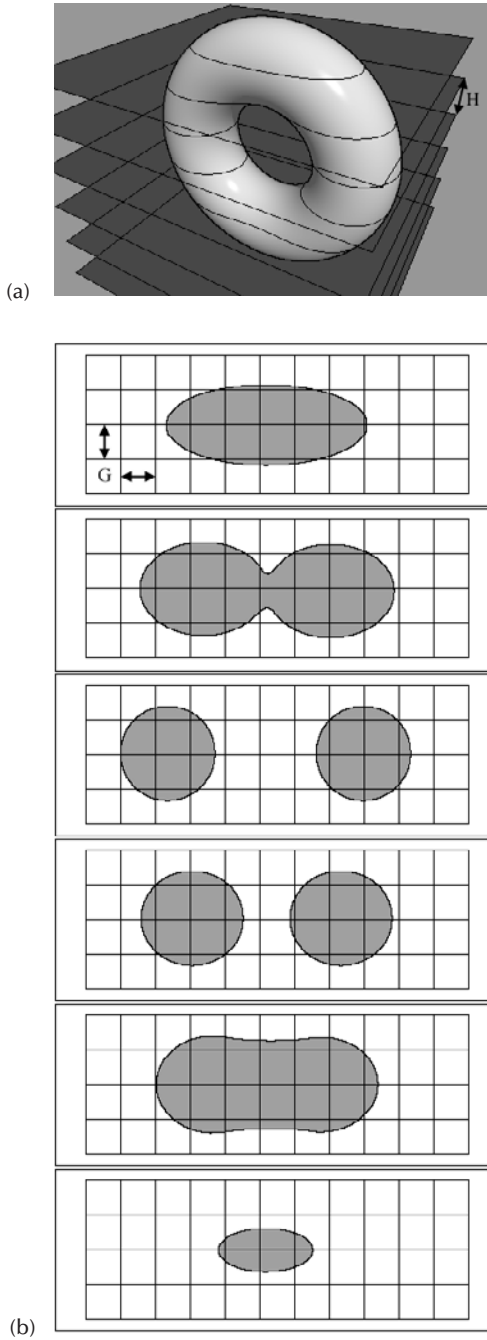


FIGURE 1.14 Illustration of the Cavalieri method for measuring an object's volume. A series of sections is cut with spacing = H and examined with a grid of spacing G . The number of points in the grid that touch the object are counted (N). The volume is then estimated as $N \cdot H \cdot G \cdot G$.

SURFACE AREA

Besides volume, the most obvious and important property of three dimensional structures is the surfaces that are present. These may be surfaces that bound a particular phase (which for this purpose includes void space or pores) and separate it from the remainder of the structure which consists of different phases, or it may be a surface between two identical phase regions, consisting of a thin membrane such as the liquid surfaces between bubbles in the head on beer. Most of the mechanical and chemical properties of foods depend in various ways on the surfaces that are present, and it is, therefore important to be able to measure them.

Just as volumes in 3D structures are revealed in 2D section images as areas where the section plane has passed through the volume, so surfaces in 3D structures are revealed by their intersections with the 2D image plane. These intersections produce lines (Figure 1.15). Sometimes the lines are evident in images as being either lighter or darker than their surroundings, and sometimes they are instead marked by a change in brightness where two phase volumes meet. Either way, they can be detected in the image either visually or by computer-based image processing and used to measure the surface area that is present.

The length of the lines in the 2D images is proportional to the amount of surface area present in 3D, but there is a geometric factor introduced by the fact that the section plane does not in general intersect the surface at right angles. It has been

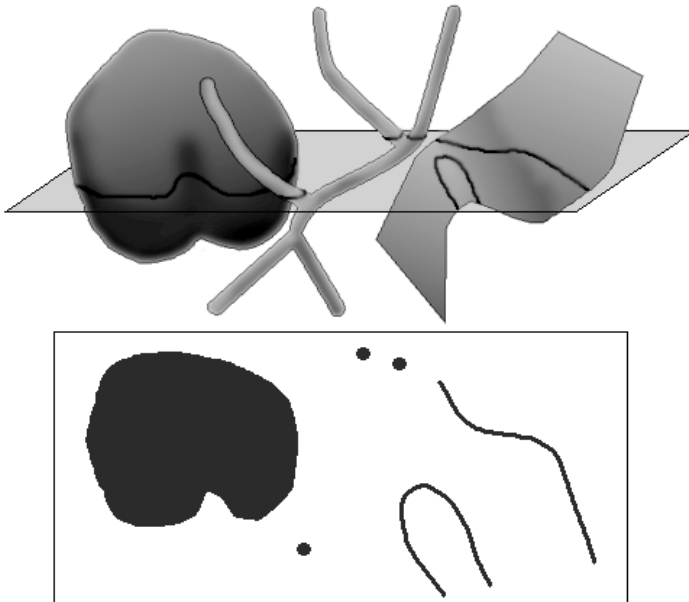


FIGURE 1.15 Passing a section plane through volumes, surfaces, and linear structures produces an image in the plane in which the volumes are shown as areas, the surfaces as lines, and the linear structures as points.

shown by stereologists that by averaging over all possible orientations, the mathematical relationship is

$$S_V = \frac{4}{\pi} \cdot B_A \quad (1.6)$$

where S_V is the area of the surface per unit volume of sample and B_A is the length of boundary line per unit area of image, where the boundary line is the line produced by the intersection of the three-dimensional surface and the section plane. The geometric constant $(4/\pi)$ compensates for the variations in orientation, but makes the tacit assumption that either the surfaces are isotropic — arranged so that all orientations are equally represented — or that the section planes have been made isotropic to properly sample the structure if it has some anisotropy or preferred orientation.

This last point is critical and often insufficiently heeded. Most structures are not isotropic. Plants have growth directions, animals have oriented muscles and bones, manufactured and processed foods have oriented structures produced by extrusion or shear. Temperature or concentration gradients, or gravity can also produce anisotropic structures. This is the norm, although at fine scales emulsions, processed gels, etc. may be sufficiently isotropic that any orientation of measurement will produce the same result. Unless it is known and shown that a structure is isotropic it is safest to assume that it is not, and to carry out sampling in such a way that unbiased results are obtained. If this is not done, the measurement results may be completely useless and misleading.

Much of the modern work in stereology has been the development of sampling strategies that provide unbiased measurements on less than ideal, anisotropic or nonuniform structures. We will introduce some of those techniques shortly.

Measuring the length of the line in a 2D image that represents the intersection of the image plane with the surface in three dimensions is difficult to do accurately, and in any case we would prefer to have a counting procedure instead of a measurement. That goal can be reached by drawing a grid of lines on the image and counting the number of intersections between the lines that represent the surface and the grid lines. The number of intersection points per length of grid line (P_L) is related to the surface area per unit volume as

$$S_V = 2 \cdot P_L \quad (1.7)$$

The geometric constant (2) compensates for the range of angles that the grid lines can make with the surface lines, as well as the orientation of the sample plane with the surface normal. This surprisingly simple-appearing relationship has been rediscovered (and republished) a number of times. Many grids, such as the one in Figure 1.12, serve double duty, with the grid points used for determining volume fraction using Equation 1.5, while the lines are used for surface area measurement using Equation 1.7.

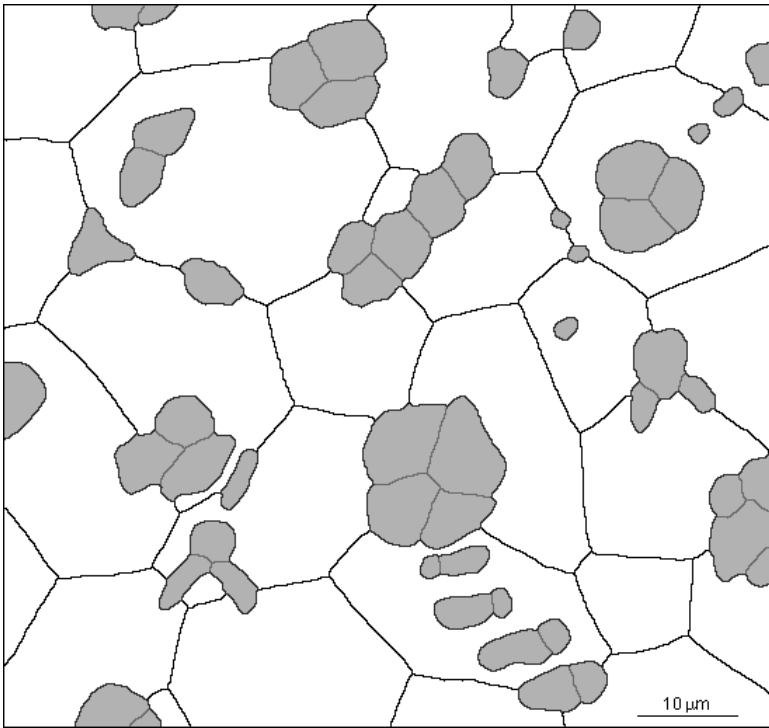
As an example of the measurement of surface area, Figure 1.16 shows an image in which the two phases (grey and white regions, respectively) have three types of interfaces — that between one white cell and another (denoted $\alpha-\alpha$), between one

grey cell and another (β - β), and between a white and a grey cell (α - β). The presence of many different phases and types of interfaces is common in food products.

By either manual procedures or by using the methods of image processing discussed in subsequent chapters, the individual phases and interfaces can be isolated and measured, grids generated, and intersections counted. Table 1.2 shows the

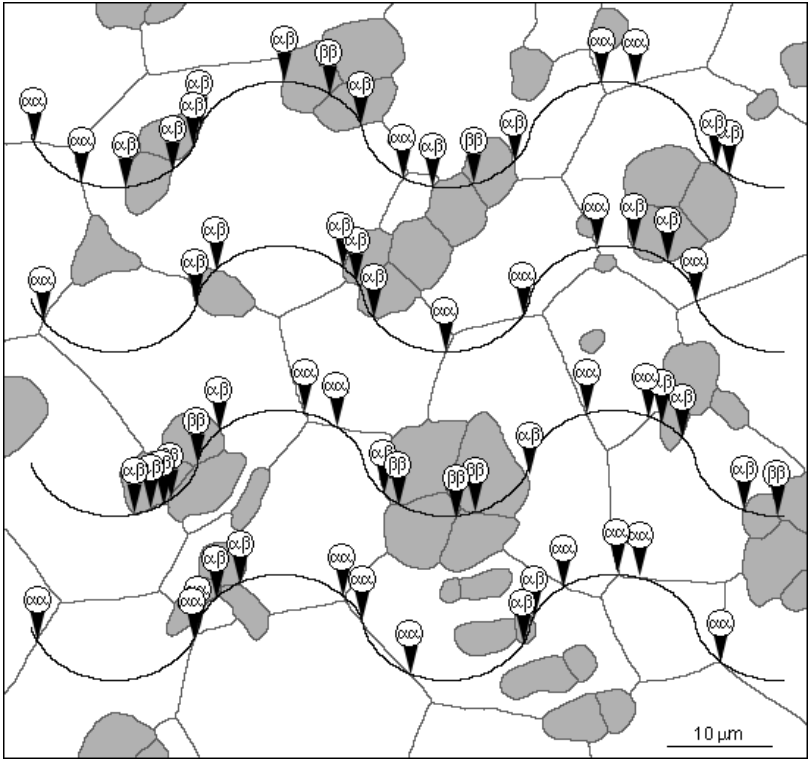
TABLE 1.2
Surface Area Measurements from Figure 1.16

| Boundary Type | Intersection Counts | Cycloid length (μm) | $S_V = 2 \cdot P_L$ (μm^{-1}) | Boundary Length (μm) | Image Area (μm^2) | $S_V = 4/\pi \cdot B_A$ (μm^{-1}) |
|---------------------|---------------------|----------------------------------|--|-----------------------------------|--------------------------------|--|
| α - α | 24 | 360 | 0.133 | 434.8 | 4500 | 0.123 |
| α - β | 29 | 360 | 0.161 | 572.5 | 4500 | 0.162 |
| β - β | 9 | 360 | 0.050 | 117.8 | 4500 | 0.033 |



(a)

FIGURE 1.16 (See color insert following page 150.) Measurement of surface area. A two-phase microstructure is measured by (a) isolating the different types of interface (shown in different colors) and measuring the length of the curved lines; and (b) generating a cycloid grid and counting the number of intersections with each type of interface. The reason for using this particular grid is discussed in the text.



(b)

FIGURE 1.16 (continued)

specific results from the measurement of the length of the various boundary lines and from the use of the particular grid shown. The numerical values of the results are not identical, but within the expected variation based on the precision of the measurements and sampling procedure used.

Note that the units of P_L , B_A and S_V are all the same (length^{-1}). This is usually reported as (area/volume), and to get a sense of how much surface area can be packed into a small volume, a value of $0.1 \mu\text{m}^{-1}$ corresponds to $100 \text{ cm}^2/\text{cm}^3$, and values for S_V substantially larger than that may be encountered. Real structures often contain enormous amounts of internal surface within relatively small volumes.

For measurement of volume fraction the image magnification was not important, because P_P , L_L , A_A and V_V are all dimensionless ratios. But for surface area it is necessary to accurately calibrate image magnification. The need for isotropic sampling is still present, of course. If the section planes have been cut with orientations that are randomized in three dimensions (which turns out to be quite complicated to do, in practice), then circles can be drawn on the images to produce isotropic sampling in three dimensions.

One approach to obtaining isotropic sampling is to cut the specimen up into many small pieces, rotate each one randomly, pick it up and cut slices in some random orientation, draw random lines on the section image, and perform the counting operations. That works, meaning that it produces results that are unbiased even if the sample is not isotropic, but it is not very efficient. A better method, developed nearly two decades ago, generates an isotropic grid in 3D by canceling out one orientational bias (produced by cutting sections) with another. It is called the method of “vertical sections” and requires being able to identify some direction in the sample (called “vertical” but only because the images are usually oriented with that direction vertical on the desk or screen). Depending on the sample, this could be the direction of extrusion, or growth, or the backbone of an animal or stem of a plant. The only criterion is that the direction be unambiguously identifiable. The method of vertical sections was one of the first of the developments in what has become known as “unbiased” or design-based stereology.

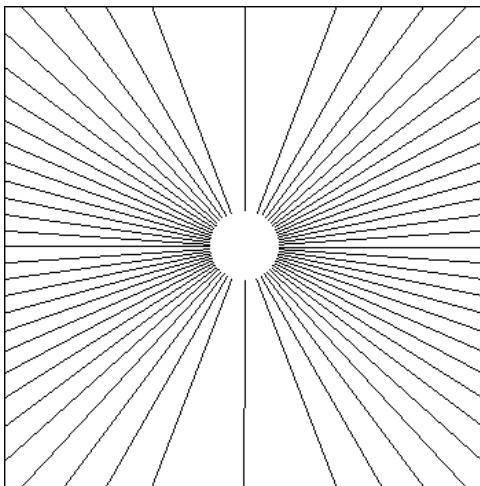
Section planes through the structure are then cut that are all parallel to the vertical direction, but rotated about it to represent all orientations with equal probability (Figure 1.17). These planes are obviously not isotropic in three-dimensional space, since they all include the vertical direction. But lines can be drawn on the section plane images that cancel this bias and which are isotropic. These lines must have sine-weighting, in other words they must be uniformly distributed over directions based not on angles but on the sines of the angles, as shown in the figure. It is possible to draw sets of straight lines that vary in this way, but the most efficient procedure to draw lines that are also uniformly distributed over the surface is to generate a set of cycloidal arcs.

The cycloid is a mathematical curve generated by rolling a circle along a line and tracing the path of a point on the rim (it can be seen as the path of a reflector on a bicycle wheel, as shown in Figure 1.18). The cycloid is exactly sine weighted and provides exactly the right directional bias in the image plane to cancel the orientational bias in cutting the vertical sections in the first place. Cycloidal arcs can be generated by a computer and superimposed on an image. The usual criteria for independent sampling apply, so the arcs should be spaced apart to intersect different bits of surface line, and not so tightly curved that they resample the same segment multiple times. They may be drawn either as a continuous line or separate arcs, as may be convenient. Figure 1.18 shows some examples.

The length of one cycloidal arc (one fourth of the full repeating pattern) is exactly twice its height (which is the diameter of the generating circle), so the total length of the grid lines is known. Counting the intersections and calculating S_V using Equation 1.7 gives the desired measure of surface area per unit volume, regardless of whether the structure is actually isotropic or not. Clearly the cutting of vertical sections and drawing of cycloids is more work than cutting sections that are all perpendicular to one direction (the way a typical microtome works) and using a simple straight-line grid to count intersections. Either method would be acceptable for an isotropic structure, but the vertical section method produces unbiased results even if the structure has preferred orientation, and regardless of what the nature of that anisotropy may be.

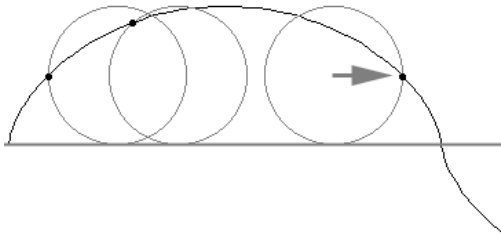


(a)

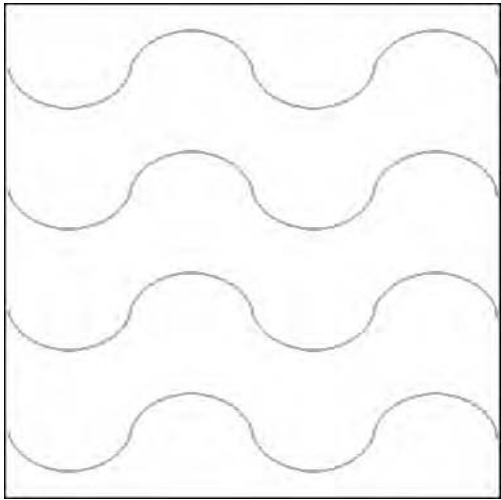


(b)

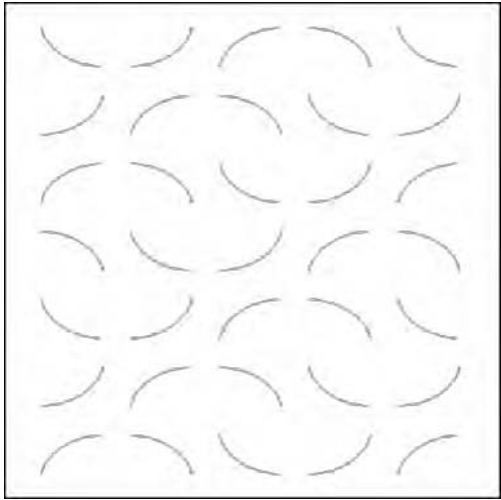
FIGURE 1.17 The method of vertical sections: (a) a series of slices are cut lying parallel to an identifiable direction, but rotated to different angles about that direction; (b) on each slice, lines that are sine-weighted (their directions incremented by equal steps in the value of the sine of the angle) are drawn. These lines isotropically sample directions in three dimensional space.



(a)



(b)



(c)

FIGURE 1.18 Cycloid grids: (a) generation of a cycloid as the path traced out by a point on the rim of a rolling circle; (b) a set of continuous cycloid grids; (c) a set of separated cycloid arcs.

LINES AND POINTS

The preceding sections have described the measurement of volumes and surfaces that may be present in 3D structures. These are, respectively, 3- and 2-dimensional features. There may also be 1- and 0-dimensional features present, namely lines and points. Surfaces were considered to include extremely thin interfaces between phases, as well as finite membranes around objects. Similarly, a linear structure may have finite thickness as long as its lateral dimensions are very small compared to its length and the size of the other structures with which it interacts. So the veins or nerves in meat, and the various kinds of fibers in either natural or man-made foods are all linear structures.

A thicker structure, such as the network of particles that form in gels (e.g., polysaccharides such as pectin or alginates), shortening and processed meats, may also be considered as a linear structure for some purposes, as can a pore network. In both cases, we imagine the lateral dimensions to shrink to form a backbone or skeleton of the network, which is then treated as linear for purposes of measurement. Note that a linear structure may consist of a single long line, many short ones, or a complex branching network. The topology of structures is considered later, at the moment only the total length is of concern.

In addition, a line exists where two surfaces meet, as indicated in Figure 1.19. One of the simplest examples of these edge lines is the structure of a bubble raft such as the head on beer. Except for the bubbles on the outside of this raft, whose surfaces are curved, all of the soap films that separate bubbles from each other are flat planes. This is the equilibrium structure of many solid materials as well, ranging from grains in metals to cells in plants. The boundaries of each facet where three planes meet are lines, and can be treated as an important component of the structure. It is these triple lines where much of the diffusion of gases and fluids occurs, for example, or which are responsible for the mechanical strength of a fiber network.

Linear structures appear as points in a section plane, where the plane intersects the line. In many real cases the lateral dimension of the linear structure is small but still large enough that the intersections appear as small features in the image. These

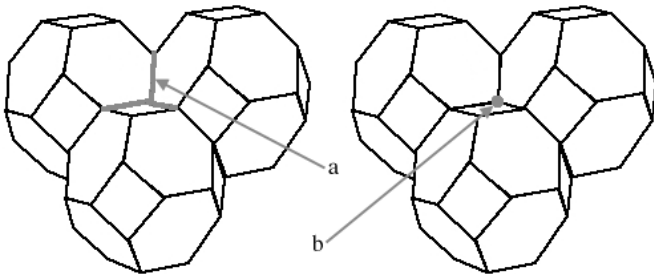


FIGURE 1.19 Diagram of a cell or bubble structure (with the topmost cell removed for clarity) showing the triple lines (a) where three cells meet and the quadruple points (b) where four cells meet.

are simply counted. The total length of the linear structure per unit volume L_V of material is calculated from the number of intersection points per unit area P_A as

$$L_V = 2 \cdot P_A \quad (1.8)$$

where P is the number of points of intersection, A is the area of the image, and (2) is a geometrical constant, as above, that compensates for the range of orientations with which the section plane can intersect the lines.

As for the measurement of surfaces, discussed above, the measurement of line length must be concerned with directionality. If the sample is not isotropic, then the probes must be. In this case the probes are the section planes, and it was noted above that producing an isotropic array of section planes is very difficult, inefficient, and wasteful of material. There is a useful technique that can use the method of vertical sections to simplify the procedure.

Thus far, measurements have been made on plane sections cut through surfaces. Either the material has been considered as opaque so that a true plane surface is examined, or in the case of transmission microscopy, the section thickness has been assumed to be very thin as compared to the dimensions of any of the structures of interest. But in many cases the food products of interest are at least somewhat transparent and it is possible to obtain images by shining radiation (light, electrons, or something more exotic) through a moderately thick slice. The resulting image shows a projection through the structure in which linear features can be seen.

Simply measuring the length of the lines will not suffice, however. There is no reason to expect them to all lie flat in the plane of the section, so that their true length can be measured, and there is likewise no reason to expect them to be isotropic in direction so that a geometric constant can be used to convert the total measured projected length to an estimate of the true length in 3D.

But another approach is possible. Imagine drawing a line on the image. That line represents a plane in the original thick slice sample that extends down through the thickness of the slice, as shown in Figure 1.20. Counting the number of intersections of the linear structure with the drawn line (which implies their intersection with the plane the line represents) gives a value of P_A (number of counts per unit area of plane). The area of the plane is just the length of the line drawn on the image times the thickness of the section, which must be known independently. Then the same relationship introduced above (Equation 1.8) can be used.

In order to obtain isotropic orientation of the plane probes (not the section planes, but the thru-the-slice planes that correspond to the lines drawn on the image), it is necessary to use the vertical sectioning approach. All of the slices are cut parallel to some assumed vertical orientation and rotated about it. Then the lines are drawn as cycloids, representing a cycloidal cylindrical surface extending down through the section thickness. Because in this case it is the orientation of the surface normals of those probe surfaces that must be made isotropic, it is necessary to rotate the grid of cycloid lines by 90 degrees on the image, as shown in Figure 1.21.

Finally, there are many structures in which the features of interest are small in dimension as compared to the scale of the image and of surrounding structures.